Fate of quasiparticles in the superconducting state

S. V. Dordevic[*]

Department of Physics, The University of Akron, Akron, Ohio 44325, USA
and Departement de Physique de la Matiere Condensee, Universite de Geneve, Quai Ernest-Ansermet 24, 1211 Geneve 4, Switzerland

D. van der Marel

Departement de Physique de la Matiere Condensee, Universite de Geneve, Quai Ernest-Ansermet 24, 1211 Geneve 4, Switzerland

C. C. Homes

Condensed Matter Physics and Materials Science Department, Brookhaven National Laboratory, Upton, New York 11973, USA

Quasiparticle properties in the superconducting state are masked by the superfluid and are not directly accessible to infrared spectroscopy. We show how one can use a Kramers–Kronig transformation to separate the quasiparticle from superfluid response and extract intrinsic quasiparticle properties in the superconducting state. We also address the issue of a narrow quasiparticle peak observed in microwave measurements, and demonstrate how it can be combined with infrared measurements to obtain a unified picture of electrodynamic properties of cuprate superconductors.

PACS number(s): 78.30.Er, 74.72.−h

I. INTRODUCTION

Infrared spectroscopy has in the past several decades become one of the premier experimental tools in condensed matter physics [1,2]. Thanks to its versatility, it has been successfully applied to essentially all types of condensed matter systems, such as superconductors, topological insulators, graphene, etc. In particular, in high-T_c cuprate superconductors, infrared based techniques have been extensively used to probe a variety of unusual and yet unresolved issues concerning their unconventional pairing state [3]. In recent years a number of attempts has been made to elucidate the properties of quasiparticles and their relaxation in the cuprates [4,5]. These attempts are based on the so-called extended-Drude model, which allows both the quasiparticles' scattering rate and their effective mass to acquire frequency dependence. These two quantities can be straightforwardly obtained from the complex optical conductivity $\tilde{\sigma}(\omega) = \sigma_1(\omega) + i\sigma_2(\omega)$ as

$$\frac{1}{\tau(\omega)} = \frac{\omega_p^2}{4\pi}\Re\left[\frac{1}{\tilde{\sigma}(\omega)}\right] = \frac{\omega_p^2}{4\pi}\frac{\sigma_1(\omega)}{\sigma_1^2(\omega) + \sigma_2^2(\omega)}, \quad (1)$$

$$\frac{m^*(\omega)}{m_b} = \frac{\omega_p^2}{4\pi}\Im\left[\frac{1}{\tilde{\sigma}(\omega)}\right]\frac{1}{\omega} = \frac{\omega_p^2}{4\pi}\frac{\sigma_2(\omega)}{\sigma_1^2(\omega) + \sigma_2^2(\omega)}\frac{1}{\omega}, \quad (2)$$

where the plasma frequency $\omega_p^2 = 4\pi e^2 n/m_b$ is usually obtained from the integration of $\sigma_1(\omega)$ up to the frequency of the onset of interband absorption:

$$\omega_p^2 = 8\int_{0+}^{\Omega}\sigma_1(\omega)d\omega. \quad (3)$$

Equations (1) and (2) are the basis of a so-called *one-component* approach [6] for the interpretation of optical properties, which assumes the existence of a single type of charge carrier in the system. Closely related quantities

are the optical self-energy $\tilde{\Sigma}^{\text{opt}}(\omega)$ [7] and memory function $\tilde{M}(\omega)$ [4,8] defined as

$$\tilde{M}(\omega) = 2\tilde{\Sigma}^{\text{opt}}(\omega) = \omega\left(\frac{m^*(\omega)}{m_b} - 1\right) + i\frac{1}{\tau(\omega)}. \quad (4)$$

As an example, in Fig. 1 we display the real and imaginary parts of the memory function $\tilde{M}(\omega)$, as well as the effective mass $m^*(\omega)/m_b$ for optimally doped $Bi_2Sr_2CaCu_2O_{8+\delta}$ (Bi2212) with $T_c = 92$ K [9], in both the normal and superconducting states. Application of Eqs. (1), (2), and (4) to the data in the superconducting state is highly problematic, even though it has been routinely done. Namely, in the superconducting state normal fluid coexists with the superfluid, and the one-component assumption is clearly violated. As was most recently pointed out by Homes *et al.* [5] this procedure cannot be used to make any reliable statements about quasiparticle properties in the superconducting state. In the superconducting state the response at microwave and far-infrared frequencies is dominated by the superfluid, causing $\sigma_2(\omega) \gg \sigma_1(\omega)$,[1] and it follows from Eq. (1) that $1/\tau(\omega) = M_2(\omega) \sim \sigma_1/\sigma_2^2$ acquires small values (see Fig. 1). Similarly, indiscriminate application of Eq. (2) to the optical conductivity in the superconducting state will result in $m^*(\omega)/m_b \sim 1/(\sigma_2\omega)$ which decreases when the superfluid forms, and $\sigma_2(\omega)$ increases (see Fig. 1).

In this work we show how to circumvent this problem, and access intrinsic quasiparticle properties in the superconducting state. The procedure expands the range of applicability of the one-component approach, and further extends the power of infrared spectroscopy. Our procedure is based on the Kramers-Kronig transformation of the optical conductivity. In the next section (Sec. II) we first present the formalism in detail. In Sec. III we apply it to model data, which serves

---

[*]dsasa@uakron.edu

---

[1]In the cuprates, the superfluid density is not as high as in conventional superconductors, resulting in $\sigma_2(\omega) > \sigma_1(\omega)$ instead of $\sigma_2(\omega) \gg \sigma_1(\omega)$. See for example Fig. 4.
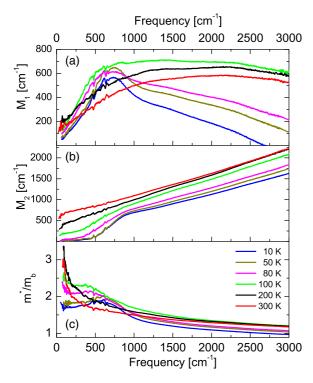
FIG. 1. (Color online) Extended-Drude analysis of optimally doped Bi2212 with $T_c = 92$ K. (a) Real part of memory function $M_1(\omega)$ obtained from Eq. (4). (b) Imaginary part of memory function $M_2(\omega)$ from Eq. (4). (c) Quasiparticle effective mass $m^*(\omega)/m_b$ calculated from Eq. (2). The values of plasma frequency ω_p used for each temperature are shown in Fig. 4(c).

to illustrate the main idea and demonstrate its usefulness. The procedure is then applied to existing infrared data on optimally doped high-T_c superconductor Bi2212 with $T_c = 92$ K (Sec. IV). We present and discuss the quasiparticle properties obtained below T_c. In this section we also address the issue of a narrow quasiparticle peak that has been observed in microwave spectroscopy, and show how it can be combined with infrared data to obtain a unified and self-consistent picture of electrodynamic properties of Bi2212. Finally, in Sec. V we summarize the most important findings made possible by the procedure.

II. KRAMERS–KRONIG APPROACH

In this section we present the details of our procedure. The approach is based on the Kramers-Kronig transformation of optical conductivity, which we introduced previously to extract the superfluid density from infrared data [10]. In the superconducting state the real part of optical conductivity can be written as

$$\sigma_1^{SC}(\omega) = \rho_s \delta(\omega) + \sigma_1^{qp}(\omega), \qquad (5)$$

where the first term on the right-hand side is the superconducting contribution and the second is the quasiparticle contribution. The corresponding imaginary part of $\sigma_1^{SC}(\omega)$ follows from a Kramers-Kronig relation:

$$\sigma_2^{SC}(\omega) = \rho_s \frac{1}{\omega} + \sigma_2^{qp}(\omega), \qquad (6)$$

where $\rho_s = \omega_s^2$ is the superfluid density or stiffness, and ω_s is the superconducting plasma frequency. The Dirac delta function in $\sigma_1^{SC}(\omega)$ is not accessible in optical data, which typically start at several meV. However, the $1/\omega$ term in $\sigma_2^{SC}(\omega)$ is mixed up with $\sigma_2^{qp}(\omega)$ and contributes to both $1/\tau(\omega)$ and $m^*(\omega)/m_b$ [Eqs. (1) and (2)]. To determine the intrinsic quasiparticle properties we must separate the two terms in Eq. (6). To that end we employ a Kramers-Kronig transformation on $\sigma_1^{qp}(\omega)$:

$$\sigma_2^{qp}(\omega) = -\frac{2\omega}{\pi} \int_{0^+}^{\infty} \frac{\sigma_1^{qp}(\omega')}{\omega'^2 - \omega^2} d\omega'. \qquad (7)$$

We emphasize that this step is completely model-independent; no *a priori* assumptions are made about the form of quasiparticle conductivity. Once $\sigma_2^{qp}(\omega)$ is calculated from Eq. (7), one can calculate the intrinsic scattering rate and effective mass in the superconducting state [Eqs. (1) and (2)] using the Kramers-Kronig-corrected $\sigma_2^{qp}(\omega)$, instead of $\sigma_2^{SC}(\omega)$. Note that $\sigma_1^{SC}(\omega)$ does not need to be corrected, as the delta function [Eq. (5)] is not accessible to optical experiments. Using the procedure described above, we can also calculate the superfluid density from Eq. (6), as was done before [10]:

$$\rho_s = \omega_s^2 = \omega\left(\sigma_2^{SC}(\omega) - \sigma_2^{qp}(\omega)\right). \qquad (8)$$

III. MODEL CALCULATIONS

To test the procedure and to demonstrate its usefulness in this section we perform the calculations on model data. We adopt a Drude model for the normal state, with the width of peak equal to 40 cm^{-1}. A BCS model for an s-wave superconductor is used in the superconducting state, and it also includes a quasiparticle peak inside the superconducting gap. The critical temperature was set at $T_c = 90$ K, and the corresponding $T = 0$ energy gap is $2\Delta = 220$ cm^{-1} (27.3 meV). Real and imaginary parts of $\tilde{\sigma}(\omega)$ are shown with thick lines at several temperatures in Figs. 2(a) and 2(b) respectively. In the superconducting state a characteristic suppression of $\sigma_1(\omega)$ is observed below the gap. The spectral weight removed from these frequencies is transferred to the delta function at zero frequency [Eq. (5)]. The values of plasma frequency are calculated from Eq. (3) and displayed in Fig. 2(c) with red circles. Note that in Eq. (3) the integral starts from 0+, which emphasizes the fact that in the superconducting state only the quasiparticle contribution should be counted towards ω_p. The upper limit of integration was set to 2000 cm^{-1}. Unlike $\sigma_1(\omega)$, $\sigma_2(\omega)$ is dominated by a characteristic $1/\omega$ response of the superfluid [Eq. (6)]. We also note that the absolute values of $\sigma_2(\omega)$ are at least an order of magnitude larger than $\sigma_1(\omega)$.

We now apply the procedure outlined in the previous section. In Fig. 2(b) with thin lines we display $\sigma_2^{qp}(\omega)$ calculated from Eq. (7). We note that these Kramers-Kronig-corrected curves are not dominated by $1/\omega$ superfluid response, but instead display a broad peak at finite frequencies, similar to the one seen at 90 K. The removal of superfluid response also reveals pronounced structure at the gap frequency, which is not observable in $\sigma_2^{SC}(\omega)$ (before the correction).

In Fig. 3 we display with blue lines the results for the real (top panels) and imaginary (bottom panels) parts of
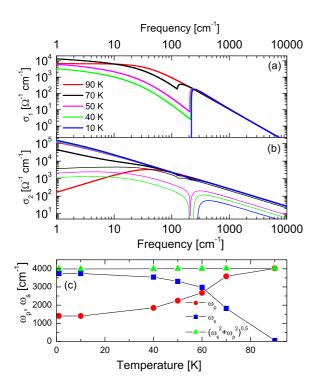
FIG. 2. (Color online) (a) Real part of the optical conductivity $\sigma_1(\omega)$ of a BCS model with $T_c = 90$ K. (b) Imaginary part of the optical conductivity $\sigma_2(\omega)$. Thick lines represent the model function, whereas thin lines of the same color represent Kramers-Kronig-corrected $\sigma_2^{qp}(\omega)$. (c) Temperature dependence of plasma frequency ω_p, superconducting plasma frequency ω_s, and the total plasma frequency $(\omega_p^2 + \omega_s^2)^{1/2}$.

the memory function $\tilde{M}(\omega)$ from Eq. (4). In the normal state both parts display constant values, typical of the Drude model. On the other hand, in the superconducting state, $M_1(\omega)$ is suppressed at higher frequencies, but does not show
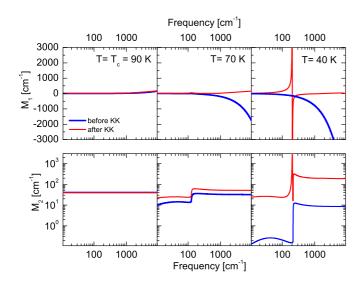

FIG. 3. (Color online) Real and imaginary parts of the memory function, $M_1(\omega)$ and $M_2(\omega)$, for the model shown in Fig. 2. The results are shown before (blue lines) and after (red lines) Kramers-Kronig correction.

any characteristic features at the gap, because the response is dominated by the superfluid. The imaginary part $M_2(\omega)$ displays characteristic suppression, especially below the gap. In the same figure we also plot with red lines the results for the memory function obtained with Kramers-Kronig-corrected $\sigma_2^{qp}(\omega)$. Expectedly, in the normal state the memory function is the same as before. However, in the superconducting state, the removal of the superfluid contribution reveals a very pronounced structure at the gap frequency in $M_1(\omega)$. The imaginary part $M_2(\omega)$ also displays structure at the gap frequency, but more importantly the suppression below the gap is much smaller than before. Above the gap $M_2(\omega)$ is enhanced compared to the normal state.

In Fig. 2(c) we display the temperature dependence of the plasma frequency ω_p (red circles) obtained from Eq. (3), and the superfluid density (blue squares) obtained from Eq. (8). As discussed above, the spectral weight removed from finite frequencies is transferred to the delta function at zero energy, but the total spectral weight must be conserved. This is indeed confirmed by Fig. 2(c) where the total (i.e., combined) plasma frequency $(\omega_p^2 + \omega_s^2)^{1/2}$ is shown with green triangles and is constant within the error bars of numerical calculations. Note that the application of Eq. (8) to the normal state data may result in a small but finite value of superconducting plasma frequency. This is due to numerical errors, and does not imply the existence of superfluid in the normal state, above T_c.

IV. Bi2212

Before applying the procedure to Bi2212, we must address the issue of a very narrow quasiparticle peak that has been observed in microwave measurements [11–13]. Its width is typically a few meV [11–13], which is outside the frequency window of typical infrared measurements. The existence of this quasiparticle peak is usually ignored during analysis of infrared data, as it does not contain a lot of spectral weight and does not significantly affect the calculation of normal state plasma frequency [Eq. (3)]. However, this narrow peak can produce a significant $1/\omega$ contribution to $\sigma_2(\omega)$, which mimics the superfluid response. If we want to calculate the London penetration depth or the superfluid stiffness, it must be separated from the superconducting contribution. We show below that in the case of optimally doped Bi2212 this can lead to correction of superconducting plasma frequency ω_s by as much as 40%.

In order to perform the integration in Eq. (7) optical conductivity data must be extended down to zero frequency. It was recently shown that because of the Kramers-Kronig relations between $\sigma_1(\omega)$ and $\sigma_2(\omega)$ one can calculate the spectral weight that is located below the lowest measured frequency [14]. However, the optical functions themselves [$\sigma_1(\omega)$ and $\sigma_2(\omega)$] cannot be retrieved without making some model assumptions about the optical spectrum. Here we will make the reasonable assumption that the quasiparticle contribution can be approximated with the Drude model, and we combine it with the microwave data on Bi2212. Figure 4 displays $\sigma_1(\omega)$ from infrared as well as the microwave values at 34.7 GHz $\simeq 1.15$ cm^{-1} (the values at 14.4 and 24.6 GHz are similar) [11]. We now fit the complex conductivity $\tilde{\sigma}(\omega)$ *simultaneously* with microwave data, imposing the constraint
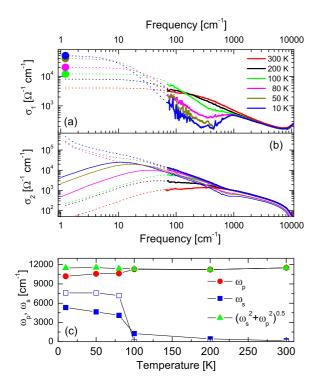
FIG. 4. (Color online) (a) Real part of the optical conductivity $\sigma_1(\omega)$ of optimally doped Bi2212 with $T_c = 92$ K. Thick lines represent the experimental data, thin dashed lines of the same color represent Drude extrapolations, and the circles represent microwave data at 34.7 GHz [11]. (b) Imaginary part of the optical conductivity $\sigma_2(\omega)$. Thick lines represent the experimental data, thin dashed lines of the same color represent Drude extrapolations, and thin lines represent Kramers-Kronig-corrected $\sigma_2^{qp}(\omega)$. (c) Temperature dependence of plasma frequency ω_p, superconducting plasma frequency ω_s, and the total plasma frequency $(\omega_p^2 + \omega_s^2)^{1/2}$. Open squares represent the values of superconducting plasma frequency ω_s obtained without Kramers-Kronig correction.

that the total spectral weight in the superconducting state is conserved.[2] In Fig. 4 the infrared data is shown with thick lines, and model fits with dotted lines. The microwave values for the corresponding temperatures are shown with the circles of the same color.

With optical conductivity extended down to zero frequency we can now apply the procedure to Bi2212 and the results are shown in Fig. 4(b) with thin lines (only below T_c). We can see that instead of a characteristic $1/\omega$ divergence, the spectra display a finite frequency peak, characteristic of quasiparticle response. The values of normal state plasma frequency ω_p and superconducting plasma frequency ω_s are shown in Fig. 4(c) with red circles and blue squares, respectively. These values are comparable with those previously reported [15]. The total plasma frequency $(\omega_p^2 + \omega_s^2)^{1/2}$ (green triangles) is within 1.5% of the normal state value. Also shown with empty squares is the superconducting plasma frequency calculated

---

[2]It was shown by Molegraaf *et al.* [16] that a fraction of spectral weight is transferred from the visible to the infrared spectral range. Note however that this effect is below the error bars of our calculations.
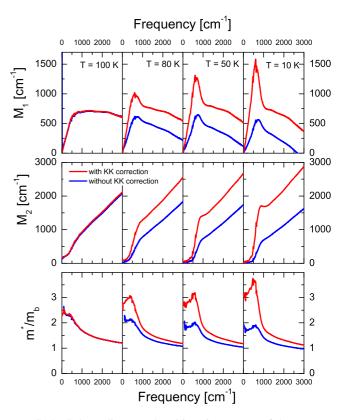

FIG. 5. (Color online) Real and imaginary parts of the memory function, $M_1(\omega)$ (top panels) and $M_2(\omega)$ (middle panels), as well as quasiparticle effective mass m^*/m_b (bottom panels) for the Bi2212 data shown in Fig. 4. The results are shown before (blue lines) and after (red lines) Kramers-Kronig correction.

using uncorrected $\sigma_2(\omega)$, which can be as much as 40% higher than the corrected one.

Once the superfluid contribution is removed from $\tilde{\sigma}(\omega)$, one can calculate intrinsic quasiparticle properties [Eqs. (1), (2), and (4)]. Figure 5 displays $M_1(\omega)$ (top panels), $M_2(\omega) = 1/\tau(\omega)$ (middle panels), and effective mass $m^*(\omega)/m_b$ (bottom panels), both before (blue lines) and after Kramers-Kronig corrections (red lines). Several selected temperatures are shown, in both the normal (100 K) and superconducting states (80, 50, and 10 K). Expectedly, optical functions in the normal state are the same before and after Kramers-Kronig correction. In the superconducting state, on the other hand, the corrections are significant and cannot be neglected. We note that even though the plasma frequency ω_p decearses in the superconducting state [Fig. 4(c)], all optical functions are *enhanced* compared to their uncorrected values. In addition, the structure at around 700 cm^{-1} is much more pronounced in all corrected spectra. The reason is the removal of superconducting contribution from $\sigma_2(\omega)$, which exposes the true quasiparticle properties.

In Fig. 6 we display the temperature dependence of quasiparticle scattering rate and effective mass, both before (blue circles) and after (red circles) Kramers-Kronig correction. The values of scattering rate were extracted as the average values at around 30 cm^{-1}. On the other hand the values of the mass were obtained from the linear fits of the low-frequency $M_1(\omega)$ spectra [Eq. (4)]. This method has proven to be more reliable than a simple extrapolation, in particular in the normal
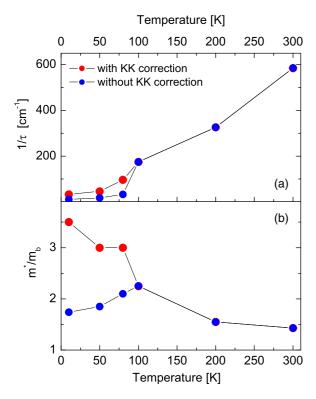
FIG. 6. (Color online) (a) Temperature dependence of scattering rate $1/\tau(\omega = 30~\text{cm}^{-1})$ before and after Kramers-Kronig correction. (b) Temperature dependence of effective mass $m^*(\omega)/m_b$ before and after Kramers-Kronig correction. These values are extracted as explained in the text. The effective mass without Kramers-Kronig correction appears to decrease in the superconducting state. However, with Kramers-Kronig correction the effective mass continues to increase below T_c, which indicates that the quasiparticles are more correlated than in the normal state.

state. The temperature dependence of scattering rate is similar before and after the correction, however the suppression of $1/\tau(\omega)$ below T_c is much less pronounced after the correction. On the other hand, the effective mass reveals dramatically different behavior. Before Kramers-Kronig correction the mass decreases in the superconducting state, as anticipated above. However, once the superfluid and the true quasiparticle properties are exposed, we can see that the effective mass actually increases as temperature decreases below T_c. This

indicates that the correlations are getting stronger in the superconducting state.

V. SUMMARY

We presented a way of calculating intrinsic quasiparticle properties, such as memory function and effective mass, in the superconducting state. The procedure allows access to the quasiparticle properties that were previously inaccessible to infrared spectroscopy. The method was first tested on model data, and then applied to infrared data on optimally doped Bi2212. The calculations have revealed that the intrinsic quasiparticle scattering rate and effective mass are enhanced in the superconducting state. In particular, the effective mass increases below T_c compared with the normal state values. This indicates that thermally excited quasiparticle in the superconducting state are more correlated than in the normal state.

We expect the method described here to be a useful tool for infrared spectroscopy, which will allow quasiparticle properties to be studied in the superconducting state. In particular, there are several issues in the cuprates that can be immediately addressed using this procedure. Scaling analysis [4,5] can now be extended below T_c, and the question of Fermi vs non-Fermi liquid quasiparticles can be studied. Another important issue is the controversy regarding the doping dependence of the quasiparticle effective mass. Namely it was recently shown using quantum oscillations [17] that the quasiparticle effective mass in $YBa_2Cu_3O_{6+x}$ in the superconducting state diverges as doping is reduced. This finding is in apparent contradiction with previous infrared measurements [18]. Using Hall data to discriminate between carrier density n and effective mass m^* contributions to infrared spectral weight, Padilla *et al.* [18] found that the effective mass in both $YBa_2Cu_3O_{6+x}$ and $La_{2-x}Sr_xCuO_4$ was constant across the phase diagram. On the other hand, by fitting a strong-coupling expressions in the normal state, van Heumen *et al.* [19] arrived at a factor of 2 decrease of the mass enhancement factor when the doping is increased from 0.1 to 0.21 holes per CuO_2 unit, in agreement with the behavior predicted from dynamical mean field theory [20]. Using the procedure outlined in this paper one can now access quasiparticle effective mass below T_c and address this important issue in the zero-temperature limit.

[1] M. Dressel and G. Gruner, *Electrodynamics of Solids* (Cambridge University Press, Cambridge, 2001).

[2] D. N. Basov, R. D. Averitt, D. van der Marel, M. Dressel, and K. Haule, Rev. Mod. Phys. **83**, 471 (2011).

[3] D. N. Basov and T. Timusk, Rev. Mod. Phys. **77**, 721 (2005).

[4] S. I. Mirzaei, D. Stricker, J. N. Hancock, C. Berthod, A. Georges, E. van Heumen, M. K. Chan, X. Zhao, Y. Li, M. Greven, N. Barisic, and D. van der Marel, Proc. Natl. Acad. Sci. **110**, 5774 (2013).

[5] C. C. Homes, J. J. Tu, J. Li, G. D. Gu, and A. Akrap, Sci. Rep. **3**, 3446 (2013).

[6] D. B. Tanner and T. Timusk, in *Physical Properties of high Temperature Superconductors III*, edited by D. M. Ginsberg (World Scientific, Singapore, 1992), p. 363, and references therein.

[7] J. Hwang, T. Timusk, and G. D. Gu, Nature (London) **427**, 714 (2004).

[8] W. Gotze and P. Wolfle, Phys. Rev. B **6**, 1226 (1972).

[9] J. J. Tu, C. C. Homes, G. D. Gu, D. N. Basov, and M. Strongin, Phys. Rev. B **66**, 144514 (2002).

[10] S. V. Dordevic, E. J. Singley, D. N. Basov, Seiki Komiya, Yoichi Ando, E. Bucher, C. C. Homes, and M. Strongin, Phys. Rev. B **65**, 134511 (2002).

[11] Shih-Fu Lee, D. C. Morgan, R. J. Ormeno, D. M. Broun, R. A. Doyle, J. R. Waldram, and K. Kadowaki, Phys. Rev. Lett. **77**, 735 (1996).

[12] D. A. Bonn, R. Liang, T. M. Riseman, D. J. Baar, D. C. Morgan, K. Zhang, P. Dosanjh, T. L. Duty, A. MacFarlane, G. D. Morris, J. H. Brewer, W. N. Hardy, C. Kallin, and A. J. Berlinsky, Phys. Rev. B **47**, 11314 (1993).

[13] T. Shibauchi, H. Kitano, A. Maeda, H. Asaoka, H. Takei, I. Shigaki, T. Kimura, K. Kishio, K. Izumi, T. Suzuki, and K. Uchinokura, J. Phys. Soc. Jpn. **65**, 3266 (1996).

[14] A. B. Kuzmenko, D. van der Marel, F. Carbone, and F. Marsiglio, New J. Phys. **9**, 229 (2007).

[15] H. L. Liu, M. A. Quijada, A. M. Zibold, Y.-D. Yoon, D. B. Tanner, G. Cao, J. E. Crow, H. Berger, G. Margaritondo, L. Forró, Beom-Hoan O, J. T. Markert, R. J. Kelley, and M. Onellion, J. Phys.: Condens. Matter **11**, 239 (1999).

[16] H. J. A. Molegraaf, C. N. Presura, D. van der Marel, P. H. Kes, and M. Li, Science **295**, 2239 (2002).

[17] S. E. Sebastian, N. Harrison, M. M. Altarawneh, C. H. Mielke, R. Liang, D. A. Bonn, W. N. Hardy, and G. G. Lonzarich, Proc. Natl. Acad. Sci. **107**, 6175 (2010).

[18] W. J. Padilla, Y. S. Lee, M. Dumm, G. Blumberg, S. Ono, K. Segawa, S. Komiya, Y. Ando, and D. N. Basov, Phys. Rev. B **72**, 060511(R) (2005).

[19] E. van Heumen, E. Muhlethaler, A. B. Kuzmenko, H. Eisaki, W. Meevasana, M. Greven, and D. van der Marel, Phys. Rev. B **79**, 184512 (2009).

[20] K. Haule and G. Kotliar, Phys. Rev. B **76**, 104509 (2007).